Erzgraber, H., Wieczorek, S., & Krauskopf, B. (2008). Bifurcations of composite-cavity modes in multi-stripe laser arrays.

Bifurcations of composite-cavity modes in multi-stripe laser arrays

Hartmut Erzgräber[a], Sebastian Wieczorek[a], and Bernd Krauskopf[b]

[a] School of Engineering, Computing and Mathematics, University of Exeter, Exeter EX4 4QF, United Kingdom

[b] Department of Engineering Mathematics, University of Bristol, Bristol BS8 1TR, United Kingdom

ABSTRACT

We consider a semiconductor laser device, where the active region consists of parallel stripes in the longitudinal direction. In the composite cavity model, the stripes are coupled via the transversal modes of the entire compound laser device. By calculating the spatial mode profiles we accurately account for the frequency detuning between the modes as well as for the gain and coupling of the individual modes, which are determined by spatial overlap integrals of the mode profiles. In particular, we show the nonlinear dependence of these quantities on the geometry of the laser device. The temporal dynamics of the composite cavity modes are described by corresponding rate equations. Bifurcation analysis of these rate equations, which are coupled to the spatial mode equations, unravels the dynamics of a twin-stripe laser. We identify different locking regions as well as regions with possibly chaotic dynamics.

Keywords: composite cavity laser, photonic lattice, coupled lasers, dynamics and bifurcations, numerical continuation

1. INTRODUCTION

Laser arrays are of broad interest because of their possible applications, for example, for high-power beam generation, frequency stabilization, as high frequency optical clocks, or for chaos generation. In many of these applications one is interested in specific dynamical properties such as continuous-wave operation, stable intensity oscillations or chaotic dynamics. Due to their versatility, semiconductor laser structures can be designed that, depending on parameters such as the coupling strength between the individual components, show all of these different dynamics.

From the fundamental point of view, coupled lasers are examples of coupled nonlinear oscillators that are well accessible experimentally. Therefore, they are studied intensively for their synchronization properties and dynamical complexity. See for example Refs. [1; 2; 3; 4] for some recent examples of the dynamical complexity observed in coupled laser systems.

The design and analysis of coupled semiconductor lasers has attracted considerably attention; see for example [5; 6; 7]. Recent technological developments allow for the fabrication of more complex and smaller semiconductor laser structures, where different geometries result in various types of optical coupling within the laser device. Specifically, in the twin-stripe laser there are two active regions separated by a passive section. The active sections are coupled via the evanescent optical field in the transversal direction. Different modelling approaches have been used, including partial differential equation models and ordinary differential equation models, with phenomenologically introduced coupling parameters; see, for example, Refs. [8; 9; 10]. In particular, simple rate equation models treat the active sections of a laser device as individual lasers, which are coupled by phenomenologically included coupling terms. Although this approach has been successfully used to reproduce experimentally observed behavior under weak coupling conditions, there are fundamental limitations of this approach due to the physically nonlinear nature of the coupling. These nonlinearities become already apparent in systems of with only two coupled active sections.

This paper investigates a compound cavity mode approach to modelling the general setup of a twin-stripe laser as shown in Figure 1. Namely, the individual stripes are coupled by the transverse modes of the entire

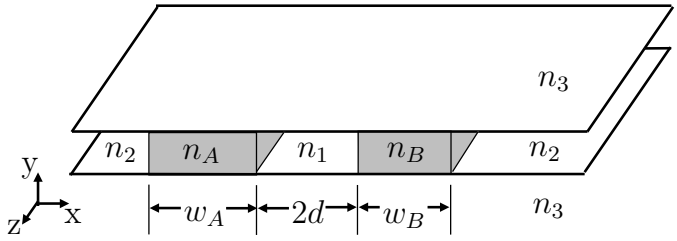

Figure 1. Sketch of the refractive index structure of a twin-stripe laser, where n_A and n_B are the refractive indices of stripe A and B, respectively. The active stripes are separated by a passive section with refractive index n_1, and surrounded by cladding layers with refractive indices n_2 and n_3, respectively.

composite-cavity system. Within the framework of semi-classical laser theory, we decompose the spatial dependence (the composite-cavity modes profiles) and the time dependence (the complex-valued electrical filed amplitude) of the laser device [11; 12]. In particular, the coupling between the different stripes is included intrinsically in the composite cavity mode structure, which makes this approach valid for arbitrary coupling. We perform a bifurcation analysis of composite cavity modes for different geometries and refractive indices of laser stripes. Such a comprehensive analysis identifies the spatio-temporal dynamics of the composite cavity modes.

This paper is structured as follows: In Section 2 we describe the modeling approach; in particular, we review the key steps that allow us to separate spatial and temporal components of the electrical field. In Section 3 we calculate the spatial mode profiles for the twin-stripe laser. This accurately determines the frequency detuning as well as the coupling and gain coefficients for the composite cavity modes as a function of the laser cavity geometry. In Section 4 we determine the locking region for the twin-stripe laser as a function of the distance $2d$ between the laser stripes and the difference Δw between the widths of the two individual laser stripes. We finish with conclusions in Section 5.

2. RATE EQUATION MODEL AND SPATIAL DEPENDENCE

In classical electrodynamics, electromagnetic radiation is described by Maxwell's equations [13]. Together with Ohm's law, Maxwell's equation can be written in a single partial differential equation for the electrical field $\vec{E}(\vec{r},t)$, which is driven by the macroscopic polarization $\vec{P}(\vec{r},t)$ of the medium,

$$\vec{\nabla}\times(\vec{\nabla}\times\vec{E})+\mu_0\sigma\frac{\partial\vec{E}}{\partial t}+\mu_0\epsilon(\vec{r})\frac{\partial^2\vec{E}}{\partial^2 t}=-\mu_0\frac{\partial^2\vec{P}}{\partial^2 t}\ . \tag{1}$$

The constants μ_0, σ, $\epsilon(\vec{r})$ are the permeability, the conductivity, and the permittivity of the medium respectively. This wave equation describes the propagation of the electric field in a medium. By assuming that there are no dipoles in the medium (apart from those induced by the electric filed) so that $\vec{\nabla}\vec{P}\approx 0$ and, hence, $\vec{\nabla}\times(\vec{\nabla}\times\vec{E})=-\nabla^2\vec{E}$, and by restricting to scalar fields, we can simplify the wave equation to

$$-\nabla^2 E(\vec{r},t)+\mu_0\sigma\frac{\partial E(\vec{r},t)}{\partial t}+\mu_0\epsilon(\vec{r})\frac{\partial^2 E(\vec{r},t)}{\partial^2 t}=-\mu_0\frac{\partial^2 P(\vec{r},t)}{\partial^2 t}\ . \tag{2}$$

This partial differential equation describes the spatio-temporal dynamics of the optical filed $E(\vec{r},t)$ and the field induced microscopic polarization $P(\vec{r},t)$. A widely-used approach to solving Eq. (2) in semi-classical laser theory is to expand the laser field as a linear superposition of the so-called composite-cavity modes. In particular, we assume that the electrical field $E(\vec{r},t)$ can be written as

$$\vec{E}(\vec{r},t)=\frac{1}{2}\sum_a \mathcal{A}_a(t)U_a(\vec{r})\ , \tag{3}$$

where $U_a(\vec{r})$ are the eigenmodes of the composite cavity; the composite-cavity modes and the subscript a refers to the index triple $a = (k, l, m)$ for the three spatial dimensions. The composite-cavity modes are solutions of the homogeneous Helmholtz equation,

$$\left[\vec{\nabla}^2 + \mu_0 \epsilon(\vec{r}) \Omega_a^2\right] U_a(\vec{r}) = 0 \ . \tag{4}$$

The spatial mode profile is determined by the spatial structure of the semiconductor; more specifically, by the boundary conditions given by the function $\epsilon(\vec{r})$. In many cases it is reasonable to assume that these boundary conditions do not change in time. Therefore, Eq. (4) can be solved independently. The solutions $U_a(\vec{r})$ form a complete set of orthogonal functions, which forms the basis of our modal expansion of the optical field. In particular, it can be shown that the $U_a(\vec{r})$ obey the orthogonality relation

$$\int_{\infty}^{\infty} d\vec{r} \epsilon(\vec{r}) U_a(\vec{r}) U_{a'}(\vec{r}) = \mathcal{N} \delta_{a,a'} \ , \tag{5}$$

where $\mathcal{N}$ is a normalization constant that can be chosen arbitrarily. In Section 3 we show the solutions of Eq. (4) for the twin-stripe laser.

Furthermore, we assume that the complex amplitude $\mathcal{A}_a(t)$ can be separated as

$$\mathcal{A}_a(t) = E_a(t) e^{-i[\nu_a t + \Phi_a(t)]} \ , \tag{6}$$

where $E_a(t)$ is the slowly varying real-valued amplitude, $\Phi_a(t)$ is the slowly varying real-valued phase of the electrical field, and ν_a is an conveniently chosen constant.

Hence, the expansion of the electrical field can be written as

$$\vec{E}(\vec{r}, t) = \frac{1}{2} \sum_a E_a(t) e^{-i[\nu_a t + \Phi_a(t)]} U_a(\vec{r}) + c.c. \ . \tag{7}$$

Similarly, the expansion for the microscopic polarization of the active medium can be written as

$$\vec{P}(\vec{r}, t) = \frac{1}{2} \sum_a \mathcal{P}_a(t) e^{-i[\nu_a t + \Phi_a(t)]} U_a(\vec{r}) + c.c. \ , \tag{8}$$

where $\mathcal{P}_a(t)$ is the complex-valued slowly varying component of the microscopic polarization associated with the ath composite cavity mode. This takes into account a possible phase shift between the optical field and induced microscopic polarization. In these equations *c.c.* stands for complex conjugation.

Inserting the expansions for the electric field and the polarization of the medium without the complex conjugate into the wave equation (2) and multiplication with $e^{i[\nu_a t + \Phi_a(t)]}$ yields

$$\begin{aligned}
&\frac{1}{2} \sum_a E_a(t) \Omega_a^2 \mu_0 \epsilon(\vec{r}) U_a(\vec{r}) \\
&+ \mu_0 \sigma \frac{1}{2} \sum_a \left[\dot{E}_a(t) - i \left[\nu_a + \dot{\Phi}_a(t)\right] E_a(t)\right] U_a(\vec{r}) \\
&+ \mu_0 \epsilon_0 \frac{1}{2} \sum_a \left[\ddot{E}_a(t) - 2i \left[\nu_a + \dot{\Phi}_a(t)\right] \dot{E}_a(t) - i E_a(t) \ddot{\Phi}_a(t) - E_a(t) \left[\nu_a + \dot{\Phi}_a(t)\right]^2\right] U_a(\vec{r}) \\
&= - \mu_0 \frac{1}{2} \sum_a \left[\ddot{\mathcal{P}}_a(t) - 2i \left[\nu_a + \dot{\Phi}_a(t)\right] \dot{\mathcal{P}}_a(t) - i \mathcal{P}_a(t) \ddot{\Phi}_a(t) - \mathcal{P}_a(t) \left[\nu_a + \dot{\Phi}_a(t)\right]^2\right] U_a(\vec{r}) \ ,
\end{aligned} \tag{9}$$

where we used the Helmholtz equation (4) in the first term. Projecting onto the passive cavity eigenmodes $U_{a'}(t)$ and integrating over the whole space yields

$$\begin{aligned}
-\dot{E}_a(t) \nu_a &= \sum_{a'} \left[E_a(t) \frac{\nu_a \sigma}{2\epsilon_0} + \frac{\nu_a^2}{2\epsilon_0} \mathrm{Im}\left[\mathcal{P}_a(t)\right]\right] \mathcal{M}_{a,a'} \\
E_a(t) \mu_0 \Omega_a^2 \mathcal{N} - E_a(t) \mu_0 \left[\nu_a + \dot{\Phi}_a(t)\right]^2 \mathcal{N} &= \sum_{a'} \frac{\mu_0 \nu_a^2}{\epsilon_0} \mathrm{Re}\left[\mathcal{P}_a(t)\right] \mathcal{M}_{a,a'} \ .
\end{aligned} \tag{10}$$

The two equations are obtained by identifying real and imaginary parts in Eq. (9). Since we assumed that $E_a(t)$, $\mathcal{P}_a(t)$, and $\Phi_a(t)$ are slowly varying in time compared to the optical frequency and that the losses are small, we neglected all terms containing $\ddot{E}_a(t)$, $\ddot{\Phi}_a(t)$, $\ddot{\mathcal{P}}_a(t)$, $\dot{E}_a(t)\dot{\Phi}_a(t)$, $\sigma\dot{E}_a(t)$, $\sigma\dot{\Phi}_a(t)$, $\dot{\Phi}_a(t)\dot{\mathcal{P}}_a(t)$, $\dot{\Phi}_a(t)\mathcal{P}_a(t)$, $\dot{\mathcal{P}}_a(t)$. Moreover, we have introduced the modal integrals,

$$\mathcal{M}_{a,a'} = \int_{\infty}^{\infty} d\vec{r} U_a(\vec{r}) U_{a'}(\vec{r}) \,. \tag{11}$$

In general, this integral is nonzero for $a \neq a'$, which means that there is always some cross-coupling between the modes. However, the off-diagonal terms are typically small and can be neglected, that is,

$$\mathcal{M}_{a,a'} \approx \mathcal{M}\delta_{a,a'} \,. \tag{12}$$

Finally, we can approximate

$$\Omega_a^2 - \left[\nu_a + \dot{\Phi}_a(t)\right]^2 = \left[\Omega_a + \nu_a + \dot{\Phi}_a(t)\right]\left[\Omega_a - \nu_a - \dot{\Phi}_a(t)\right] \approx 2\nu_a \left[\Omega_a \ - \nu_a - \dot{\Phi}_a(t)\right] \,. \tag{13}$$

These simplifications allow us to write a set first-order nonlinear differential equations determining the dynamics of the slowly varying real-valued amplitude and the slowly varying real-valued phase of the electrical field, namely

$$\begin{aligned} \dot{E}_a(t) &= -\frac{\sigma}{2\epsilon_0} E_a(t) - \frac{\nu_a}{2\epsilon_0} \mathrm{Im}\left[\mathcal{P}_a(t)\right] \frac{\mathcal{M}}{\mathcal{N}} \,, \\ \dot{\Phi}_a(t) &= (\Omega_a - \nu_a) - \frac{\nu_a}{2\epsilon_0} \frac{\mathrm{Re}\left[\mathcal{P}_a(t)\right]}{E_a(t)} \frac{\mathcal{M}}{\mathcal{N}} \,. \end{aligned} \tag{14}$$

Compare, for example, with [14, p. 237] or [15, p. 100]. It should be noted that Eq. (14) contains the eigenfrequency Ω_n of the nth compound cavity mode, which requires solving Eq. (4).

In the remaining part of this section we give equations for the microscopic polarization $P(\vec{r}, t)$. For a quantum-mechanical two-level system the equation of motion for the ath polarization mode can be written as

$$\dot{\mathcal{P}}_a(t) = \left[i(\nu_a - \omega) - \Gamma_P\right]\mathcal{P}_a(t) - \frac{i\mu_{ab}^2}{\hbar} \sum_{a'} E_{a'}(t) e^{-i\Psi_{aa'}(t)} \sum_{S_i} \epsilon^{(S_i)} N^{(S_i)}(t) \int_{\mathcal{S}_i} d\vec{r} U_a(\vec{r}) U_{a'}(\vec{r}) \,, \tag{15}$$

where ω is the transition frequency, Γ_P the polarization decay rate, μ_{ab} the dipole transition matrix element, and $\Psi_{aa'}(t) = (\nu_a - \nu_{a'})t + \Phi_a(t) - \Phi_{a'}(t)$; see for example Ref. [16]. In Eq. (15) $\mathcal{S}_i$ refers to the active stripes of the laser device, *i.e.*, the summation goes over all stripes and the integration over the area of stripe $\mathcal{S}_i$. Finally, we have introduced the population inversion $N^{\mathcal{S}_i}(t)$ within stripe $\mathcal{S}_i$, where we assume that $N^{\mathcal{S}_i}(t)$ has no spatial dependence. The dynamics of the population inversion within the S_ith stripe is given by

$$\dot{N}^{S_i}(t) = \Lambda^{(S_i)} - \Gamma_N N^{S_i}(t) + \frac{1}{\hbar} \sum_a E_a(t) \mathrm{Im}\left[\mathcal{P}_a(t)\right] \,. \tag{16}$$

Here $\Lambda^{(S_i)}$ is the pump rate and Γ_N the decay rate of the population inversion, which we assume to be constant for the whole laser device.

Taken together, Eqs. (4) and (14)–(16) describe the dynamics of the multi-stripe laser array in the so-called *class-C* laser approximation. More specifically, for semiconductor lasers the polarization decay rate Γ_P is much larger than the decay rates of the optical field Γ_E, and the inversion Γ_N. This allows for adiabatic elimination of the polarization, *i.e.*, the time dependence of the polarization $P(t)$ can be obtained directly from Eq. (15). Finally, in order to properly model a semiconductor laser device, we have to identify the local gain and refractive index changes in Eqs. (15) and replace them with the phenomenological formulas for semiconductor material.

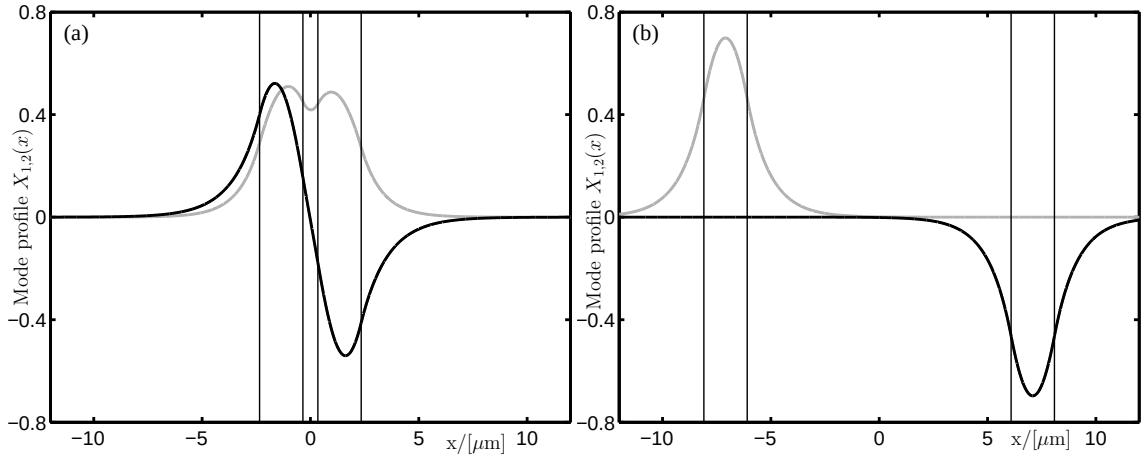

Figure 2. Mode profiles for the same refractive index difference ($n_B - n_A$), but different distances between the laser channels; specifically for $n_B = 3.47$, $n_A = 3.4711$, $d = 0.36$ in panel (a), and $n_B = 3.47$, $n_A = 3.4711$, $d = 6.09$ in panel (b).

Casting the equations in dimensionless form and restricting to two active stripes, we can write the model equations as

$$\begin{aligned}
\dot{E}_n &= -\gamma E_n + \gamma \sum_{k=1,2} \left\{ \sum_{S_i=A,B} \left[C_{kn}^{S_i}(1+\beta N^{S_i}) \cos(\Phi_{kn}) - \beta C_{kn}^{S_i} \alpha^{S_i}(1+N^{S_i}) \sin(\Phi_{kn}) \right] \right\} E_k \ , \\
\dot{\Phi}_n &= \Omega_n + \gamma \sum_{k=1,2} \left\{ \sum_{S_i=A,B} \left[\beta C_{kn}^{S_i} \alpha^{S_i}(1+N^{S_i}) \cos(\Phi_{kn}) + \beta C_{kn}^{S_i}(1+\beta N^{S_i}) \sin(\Phi_{kn}) \right] \right\} \frac{E_k}{E_n} \ , \\
\dot{N}_{\mathcal{S}_i} &= \Lambda_{\mathcal{S}_i} - (N_{\mathcal{S}_i}+1) - \sum_{n,m} C_{nm}^{\mathcal{S}_i}(1+\beta N_{\mathcal{S}_i}) \cos(\Phi_{nm}) E_m E_n \ .
\end{aligned} \tag{17}$$

In Eqs. (17) time t is rescaled with respect to the carrier decay time; compare with Ref. [17]. The remaining dimensionless parameters are the linewidth enhancement factor α, the pump parameter Λ, the gain coefficient β, and the ratio $\gamma = \Gamma_E/(2\Gamma_N)$ of the optical field and population decay rates. We assume that all these parameters are identical for both stripes, and we set them to realistic values of $\alpha = 3.0$, $\Lambda = 2.0$, $\beta = 8.4087$, and $\gamma = 10.0$. Furthermore, the constants $C_{kn}^{S_i}$ describe the modal integrals

$$C_{kn}^{S_i} = \frac{n_{\mathcal{S}_i}^2}{\mathcal{N}} \int_{\mathcal{S}_i} dx X_k(x) X_n(x) \, . \tag{18}$$

They can be reduced to one dimension, where $X_k(x)$ represent the mode profiles in the lateral x-direction; see Eq. (19). This require solving the spatial mode problem given by Eq. (4).

3. COMPOUND LASER MODES

The twin-stripe laser consists of two active regions — two stripes A and B parallel to each other. The stripes can differ in their transversal geometry and in their respective refractive indices. Figure 1 shows a sketch of the refractive index structure of a twin-stripe laser.

Because of the geometry of the twin-stripe laser we can assume, that the solutions $U_a(\vec{r})$ of the homogeneous Helmholtz equation (4) can be factorized as

$$U_{k,l,m}(\vec{r}) = X_k(x) Y_l(y) Z_m(z) \ . \tag{19}$$

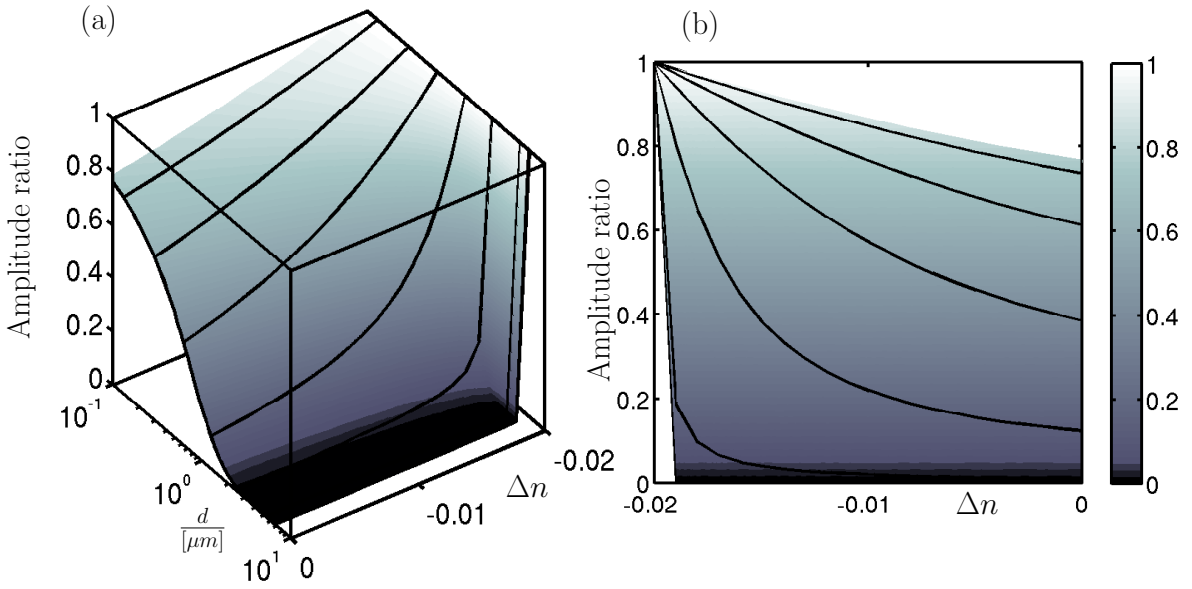

Figure 3. Ratio between the amplitudes of the two lowest-order modes in the plane of refractive index difference Δn and transversal distance d between the two stripes.

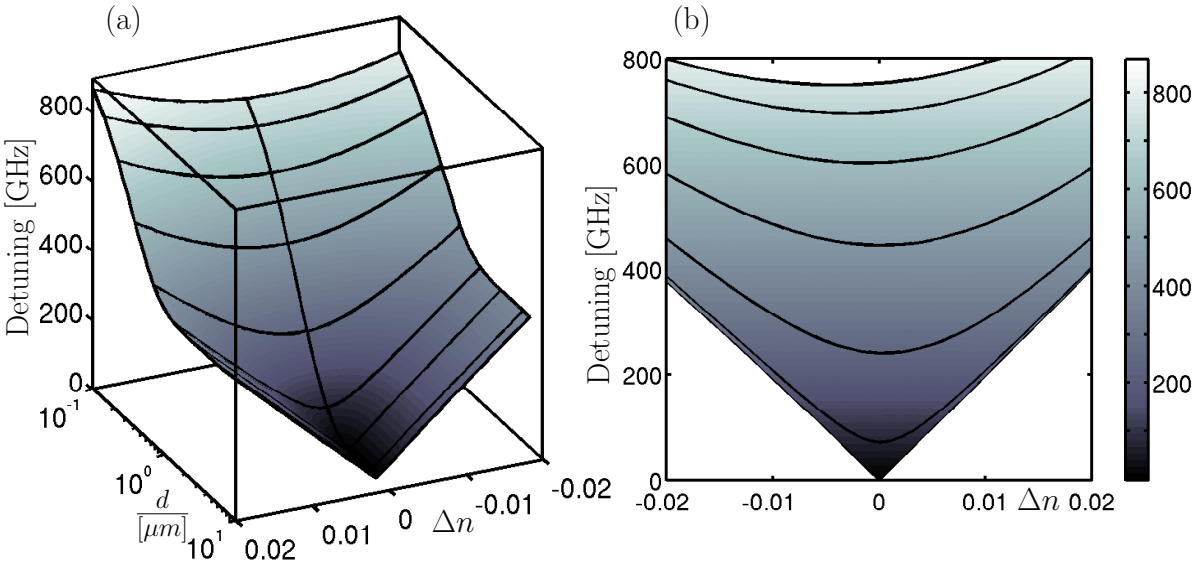

Figure 4. Frequency detuning between the two lowest-order modes in the plane of refractive index difference Δn and transversal distance d between the two stripes.

By substituting this ansatz into the Helmholtz equation we get

$$\frac{1}{X_k}\frac{\partial^2 X_k}{\partial x^2}+\frac{1}{Y_l}\frac{\partial^2 Y_l}{\partial y^2}+\frac{1}{Z_m}\frac{\partial^2 Z_m}{\partial z^2}+\mu\epsilon(x)\Omega^2_{k,l,m}=0\,, \tag{20}$$

which can be separated into the x-, y- and z-components, yielding

$$\begin{aligned}\left[\frac{\partial^2 Z}{\partial z^2}+k_z^2\right]Z(z)&=0\,,\\ \left[\frac{\partial^2 Y}{\partial y^2}+n^2(y)k_y^2\right]Y(y)&=0\,,\\ \left[\frac{\partial^2 X}{\partial x^2}+k^2n^2(x)-k_z^2\right]X(x)&=0\,.\end{aligned} \tag{21}$$

In particular, for the y-, and z-directions we assume single mode operation, with the lowest-order mode in the y-direction. In case of an edge emitting laser the wave number in the z-direction (longitudinal direction) is typically on the order of a few hundred.

For the x-direction, however, we have to solve the boundary value problem, where $n(x)$ describes the variations of the refractive index in the x-direction. For a laser device with two stripes we make the following ansatz

$$X(x)=\begin{cases} Ge^{p_2(x+d+w_A)} & \text{if} \quad x\le -d-w_A\,,\\ A\sin\left[p_A(x+d+w_A)\right]+B\cos\left[p_A(x+d+w_A)\right] & \text{if} \quad -d-w_A<x\le -d\,,\\ Ce^{-p_1(x+d)}+De^{p_1(x-d)} & \text{if} \quad -d<x\le d\,,\\ E\sin\left[p_B(x-d)\right]+F\cos\left[p_B(x-d)\right] & \text{if} \quad d<x\le d+w_B\,,\\ He^{-p_2(x-d-w_B)} & \text{if} \quad d+w_B\le x\,.\end{cases} \tag{22}$$

Ansatz (22) gives the conditions for the constants p_1, p_2, p_A, and p_B, namely

$$\begin{aligned}p_2^2+n_2^2k^2-\beta^2&=0\,,\\ -p_A^2+n_A^2k^2-\beta^2&=0\,,\\ p_1^2+n_1^2k^2-\beta^2&=0\,,\\ -p_B^2+n_B^2k^2-\beta^2&=0\,.\end{aligned} \tag{23}$$

The amplitudes A–G are determined from the requirement that $X(x)$ is continuous, yielding

$$\begin{array}{llrcl}\text{at} & x=-d_A: & G & = & B\,,\\ \text{at} & x=-d: & A\sin\left(p_Aw_A\right)+B\cos\left(p_Aw_A\right) & = & C+De^{-2dp_1}\,,\\ \text{at} & x=d: & Ce^{-2dp_1}+D & = & F\,,\\ \text{at} & x=d_B: & E\sin\left(p_Bw_B\right)+F\cos\left(p_Bw_B\right) & = & H\,,\end{array} \tag{24}$$

and that $\frac{dX}{dx}$ is continuous, yielding

$$\begin{array}{llrcl}\text{at} & x=-d_A: & p_2G & = & p_AA\,,\\ \text{at} & x=-d: & p_A\left[A\sin\left(p_Aw_A\right)-B\cos\left(p_Aw_A\right)\right] & = & p_1\left[-C+De^{-2dp_1}\right]\,,\\ \text{at} & x=d: & p_1\left[-Ce^{-2dp_1}+D\right] & = & p_BF\,,\\ \text{at} & x=d_B: & p_B\left[E\sin\left(p_Bw_B\right)-F\cos\left(p_Bw_B\right)\right] & = & -p_2H\,.\end{array} \tag{25}$$

Hence, the compound-cavity mode amplitudes A–G can be determined successively

$$
\begin{aligned}
G &= \mathcal{N}\,, \\
A &= \frac{p_2}{p_A} G\,, \\
B &= G\,, \\
C &= -\frac{p_A}{2p_1}\left[A\cos\left(w_A p_A\right) - B\sin\left(w_A p_A\right)\right] - \frac{1}{2}\left[A\sin\left(w_A p_A\right) - B\cos\left(w_A p_A\right)\right]\,, \\
D &= \frac{1}{2} e^{2dp_1}\left\{\left[A - \frac{p_A}{p_1}B\right]\sin\left(w_A p_A\right) - \left[\frac{p_A}{p_1}A + B\right]\cos\left(w_A p_A\right)\right\}\,, \\
E &= \frac{p_1}{p_B}\left[D - Ce^{-2dp_1}\right]\,, \\
F &= Ce^{-2dp_1} + D \\
H &= -\frac{p_B}{p_2}\left[E\sin\left(w_B p_B\right) + F\cos\left(w_B p_B\right)\right]\,,
\end{aligned}
\tag{26}
$$

whereas the propagation constants are determined by the transcendental equation

$$
F\left[\frac{p_B}{p_2}\sin\left(p_B w_B\right) - \cos\left(p_B w_B\right)\right] = E\left[\frac{p_B}{p_2}\cos\left(p_B w_B\right) - \sin\left(p_B w_B\right)\right]\,. \tag{27}
$$

Equations (26) and (27) have to be solved numerically to determine the frequency Ω_n of the nth compound cavity mode and its amplitudes A–G.

For the two-stripe laser the two lowest-order modes for different distances d between the stripes are shown in Figure 2; the values for the refractive indices are given in the figure caption. In Figure 2 the gray curve corresponds to the mode with the low frequency, whereas the black curve is the mode with high frequency. Since there is a small mismatch between the refractive indices of the two stripes, the mode profiles are not exactly symmetric or anti-symmetric. For small distance d the overlap between the modes, and therefore the coupling, is rather large; see Figure 2(a). Furthermore, it can be seen that the amplitudes of the same mode in the different stripes have almost the same magnitudes. In the limit $d \to 0$ the composite-cavity modes become the modes of a single large cavity. On the other hand, if the distance d between the stripes is large, which means that the coupling between them is small, the modes are concentrated in a single stripe. This can be seen in Figure 2(b), where mode 1 is concentrated in stripe A and mode 2 is concentrated in stripe B. In the limit $d \to \infty$ the composite cavity modes become the modes of two individual uncoupled lasers.

Figure 3 shows the ratio between the amplitudes of the two lowest-order modes in stripe A in the plane of transversal distance d and refractive index mismatch Δn between the laser stripes. This ratio can be interpreted as an estimation for the coupling strength between the two modes. It can be seen that the coupling depends nonlinearly on both: d and Δn. In particular, for large distances d, the coupling immediately drops to zero for $\Delta n \neq 0$. This situation corresponds to two individual uncoupled modes. Since, the two modes are located in the two different laser stripes, again this can be interpreted as two individual uncoupled lasers. On the other hand, for small distances the ratio between the amplitudes decreases only slowly with $|\Delta n|$. In this case the coupling is rather strong which leads to comparable magnitudes of the mode amplitudes in the different stripes over a long interval of refractive index differences $(n_B - n_A)$.

4. LOCKING REGION

As we have seen in the previous section the mode profiles and therefore the frequency detuning as well as the coupling and gain coefficients which are determined by the modal integrals Eq. (18) depend nonlinearly on the geometry of the laser device. Thus, in order to accurately account for these dependencies, the rate equation model Eq. (17) for the total optical field and inversion of the laser device needs to be solved simultaneously with the modal problem Eqs. (23), (26) and (27). To reveal the bifurcation structure and the dynamics of this system we use numerical continuation with AUTO [18].

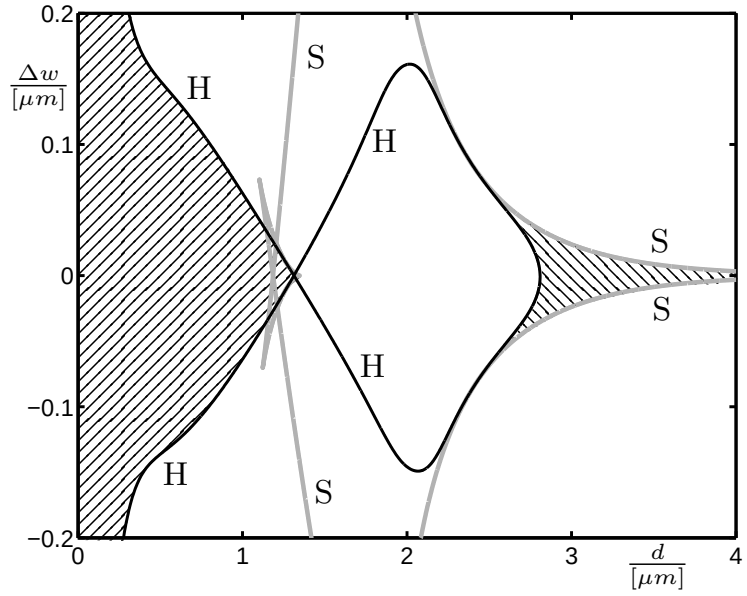

Figure 5. Two-parameter bifurcation diagram in the plane of transversal distance d and detuning Δw between the two stripes. The hatched regions indicate stable locking, and the curves are saddle-node bifurcation (S) and Hopf bifurcations (H) as labeled.

Figure 5 shows a two-parameter bifurcation diagram, where the transversal distance d and the detuning Δw between the stripes are the free parameters. It should be noted that changing these parameters change the frequencies Ω_n and the coupling coefficients $C_{kn}^{S_i}$, which need to be determined from the set of transcendental equation for the spatial mode profiles Eqs. (23), (26) and (27). The hatched regions in Figure 5 indicate stable continuous-wave (cw) emission of the laser device. These regions are bound by saddle-node (S) bifurcations and Hopf (H) bifurcations as labeled in the figure. In particular, there is a stable region for small distances d — small d corresponds to strong coupling between the modes. In this region there is only one dominant mode and the laser emits in this mode. As d is increased this cw-state undergoes a Hopf bifurcation which for large detuning Δw, leads to beating between the two modes. There is a second region of stable cw-emission for large d. In this region both modes have comparable intensities and are phase locked. This region is bound by saddle-node bifurcations towards increasing $|\Delta w|$ and by a Hopf bifurcation towards decreasing d. These two regions of stable cw-emission are separated by a region of complicated dynamics for intermediate values of d. A comprehensive study of the bifurcation structure, also in dependence on other parameters such as the linewidth enhancement factor α, is the subject of ongoing research.

5. CONCLUSIONS

We have investigated the dynamics of a laterally coupled semiconductor laser structure — the so-called *twin-stripe laser*. In the framework of semi-classical laser theory we considered a compound cavity mode model, which accurately takes into account the spatial structure, and the resulting frequency detuning and the coupling coefficients for each compound cavity mode. The temporal dynamics for each mode is determined by rate equations for the modal fields and the inversions of the stripes. We showed, that the compound cavity mode frequency as well as the gain and coupling coefficients depend nonlinearly on the geometry of the stripes and the distance between them. This shows the need for a composite cavity mode model which, intrinsically takes these effects into account.

A bifurcation analysis of the composite cavity mode model was performed to determine the dynamics of the twin-stripe laser. In particular, we found two distinct regions with stable continuous-wave emission: one

for small distances and on for large distances between the stripes. Further investigation of the dynamics of this system will concentrate on the overall bifurcation structure, which will reveal in more detail parameter regions of stable as well as of complex dynamics of the twin-stripe laser.

ACKNOWLEDGMENTS

This research was supported by Great Western Research Fellowship 18 "Modelling and nonlinear dynamics of optical nanodevices: nanolasers and photonic nanocircuits."

References

[1] D. J. DeShazer, R. Breban, E. Ott, and R. Roy, "Detecting phase synchronization in a chaotic laser array," *Phys. Rev. Lett.* **87**, p. 044101, Jul 2001.

[2] S. Wieczorek and W. W. Chow, "Chaos in practically isolated microcavity lasers," *Physical Review Letters* **92**(21), p. 213901, 2004.

[3] H. Erzgräber, D. Lenstra, B. Krauskopf, E. Wille, M. Peil, I. Fischer, and W. Elsäßer, "Mutually delay-coupled semiconductor lasers: Mode bifurcation scenarios," *Opt. Commun.* **255(4-6)**, pp. 286–296, 2005.

[4] H.-J. Wünsche, S. Bauer, J. Kreissl, O. Ushakov, N. Korneyev, F. Henneberger, E. Wille, H. Erzgräber, M. Peil, W. Elsäßer, and I. Fischer, "Synchronization of delay-coupled oscillators: A study on semiconductor lasers," *Phys. Rev. Lett.* **94**, p. 163901, 2005.

[5] L. A. Coldren and T. Koch, "Analysis and design of coupled-cavity lasers – part i: Threshold gain analysis and design guidelines," *IEEE J. Quantum Electron* **QE-20(6)**, pp. 659–670, 1984.

[6] L. A. Coldren and T. Koch, "Analysis and design of coupled-cavity lasers – part ii: Transient analysis," *IEEE J. Quatum Electron* **QE-20(6)**, pp. 671–682, 1984.

[7] D. Botez and D. Scifres, eds., *Diode Laser Arrays*, Cambridge University Press, 1994.

[8] O. Hess and E. Schöll, "Spatio-temporal dynamics in twin-stripe semiconductor lasers," *Physica D: Nonlinear Phenomena* **70**, pp. 165–177, Jan. 1994.

[9] O. Hess and E. Schöll, "Eigenmodes of the dynamically coupled twin-stripe semiconductor laser," *Phys. Rev. A* **50**, pp. 787–792, Jul 1994.

[10] P. De Jagher, M. Yousefi, and D. Lenstra, "A 2-oscillator model for the twin-stripe cavity," in *Proceedings of SPIE*, 2003.

[11] S. A. Shakir and W. W. Chow, "Semiclassical theory of coupled lasers," *Opt. Lett.* **9**(6), p. 202, 1984.

[12] S. A. Shakir and W. W. Chow, "Semiclassical theory of coupled lasers," *Phys. Rev. A* **32**, pp. 983–991, Aug 1985.

[13] J. D. Jackson, *Classical Electrodynamics*, John Wiley & Sons, Inc, 1999.

[14] W. Chow and S. Koch, *Semiconductor-Laser Fundamentals*, Springer-Verlag, Berlin, 1999.

[15] M. Sargent III, M. Scully, and W. Lamb, *Laser Physics*, Addison-Wesley, New York, 1974.

[16] S. Wieczorek and W. W. Chow, "Bifurcations and interacting modes in coupled lasers: A strong-coupling theory," *Physical Review A (Atomic, Molecular, and Optical Physics)* **69**(3), p. 033811, 2004.

[17] S. Wieczorek and W. W. Chow, "Global view of nonlinear dynamics in coupled-cavity lasers — a bifurcation study," *Optics Communications* **246**, pp. 471–493, Feb. 2005.

[18] E. Doedel, A. Champneys, T. Fairgrieve, Y. Kuznetsov, B. Oldeman, R. Paffenroth, B. Sandstede, X. Wang, and C. Zhang, "AUTO-07P: continuation and bifurcation software for ordinary differential equations," tech. rep., Concordia University, Montreal, Canada, 2007.